Applied Catalysis A: General 450 (2013) 178–188

Contents lists available at SciVerse ScienceDirect

Applied Catalysis A: General

journal homepage: www.elsevier.com/locate/apcata

Establishing the role of Brønsted acidity and porosity for the catalytic etherification of glycerol with tert-butanol by modifying zeolites

María Dolores González, Yolanda Cesteros*, Pilar Salagre

Departament de Química Física i Inorgànica, Universitat Rovira i Virgili, C/Marcel lí Domingo s/n, 43007 Tarragona, Spain

ARTICLE INFO

Article history:
Received 16 March 2012
Received in revised form
28 September 2012
Accepted 11 October 2012
Available online 7 November 2012

Keywords:
Glycerol etherification
Zeolite
Fluorination
Desilication
Dealumination
Tert-butanol
Brønsted acid sites
Porosity

ABSTRACT

The role of Brønsted acidity and porosity for the etherification of glycerol with tert-butanol was studied by modifying the surface and acidic characteristics of three commercial Na-zeolites (mordenite, beta and ZSM-5) by protonation, dealumination, desilication-protonation, lanthanum-exchange and fluorination. Catalytic results can be related to the amount and strength of Brønsted acid sites together with the accessibility of the reactants to the acid sites. Modifications made on ZSM-5 did not affect considerably its surface and acidic properties, and consequently its catalytic behaviour, leading moderate conversion values and low/null selectivity to di- and tri-tertiary butyl ethers of glycerol (h-GTBE). Mordenite catalysts showed low conversion and moderate/low selectivity to h-GTBE due to the lower amount of acid centres, lower external surface area, more hydrophilic character and lower dimensionality of the mordenite structure when compared with the other two zeolites. Beta catalysts exhibited the best catalytic results. The introduction of fluorine in the beta zeolite framework generated higher amounts of stronger acid sites, which were able to transform glycerol until the glycerol triether. Thus, fluorinated beta yielded the best conversion (75%) and selectivity to h-GTBE (37%) with the formation of glycerol triether in low amounts. These values were comparable to those obtained at the same reaction conditions with an Amberlyst-15, an acid catalyst traditionally used for this reaction.

1. Introduction

Glycerine (glycerol or 1,2,3-propanetriol) has over 1500 known end uses, including applications in cosmetics, pharmaceuticals and food products [1,2]. During biodiesel manufacture, by transesterification of vegetable oils with methanol, glycerine is formed as by-product (10 wt.% of the total product) [1–3]. The price of glycerol is falling as fast as biodiesel plants are being built. Research is currently starting to find new outlets to convert the surplus of glycerol into high-added value products that improve the economy of the whole process [1,4–8].

One challenging option is the catalytic etherification of glycerol with tert-butanol or isobutene to obtain di- and tri-tertiary butyl ethers of glycerol (h-GTBE), which is an excellent additive with a large potential for diesel and biodiesel reformulation [9–11]. Thus, when h-GTBE was incorporated in standard 30–40% aromatic-containing diesel fuel, emissions of particulate matter, hydrocarbons, carbon monoxide, and unregulated aldehydes decreased significantly [10,11]. Besides, h-GTBE can replace methyl tertiary butyl ether (MTBE), which is used as valuable additive because of their antidetonant and octane-improving properties, but is detrimental to the environment.

Etherification of glycerol with isobutylene (IB) or with tertiary butanol (TBA) has been studied in the presence of acid catalysts [12–21]. Etherification with isobutene yielded to better conversion and better selectivity values to h-GTBE than etherification with tert-butanol [14,16]. The water formed when using TBA as reagent seems to have an inhibition effect on glycerol terbutylation. However, the use of tert-butanol, as both reactant and glycerol solvent, instead of gaseous isobutylene, overcomes the technological problems arising from the need to use solvents able to dissolve glycerol (i.e. dioxane, dimethyl sulfoxide) and typical drawbacks of a complex three-phase system (mass transfer phenomena) [14,22]. Also, the simpler reaction system with tert-butanol can be very useful to the systematic study of new catalytic systems.

There are few studies about the catalytic etherification of glycerol with tert-butanol [13,14,23–25]. Klepáčová et al. reported that acidic resin catalysts (Amberlyst type) exhibited higher conversion (88%) than zeolites H-Y and H-Beta but, on the whole, low selectivity to h-GTBE (around 25%) was achieved for this reaction, which were performed in a batch reactor at 338 K with a TBA/glycerol ratio of 4, at reaction times of 300 min [13,14]. It is important to note that glycerol triether was not detected when using these H-zeolites. This has been attributed to steric hindrance effects because

* Corresponding author. Tel.: +34 977558785; fax: +34 977559563.
E-mail addresses: yolanda.cesteros@urv.cat, yolanda.cesteros@urv.net (Y. Cesteros).

0926-860X/$ – see front matter © 2012 Elsevier B.V. All rights reserved.
http://dx.doi.org/10.1016/j.apcata.2012.10.028

of the microporosity of the zeolites [14]. Luque et al. evaluated a new family of mesoporous carbonaceous materials, denoted as Starbon, as catalysts for this reaction. Etherification reaction was carried out in a microwave-irradiated tube under continuous stirring for short time periods. The authors reported a conversion of 66% with almost total selectivity to the monoether [23]. Frusteri et al. did not improve the catalytic results of Amberlyst when using lab-made silica supported acid catalysts [24]. More recently, Ozbay et al. studied this reaction in a flow reactor at short residence time using Amberlyst, Nafion and alumina catalysts [25]. Again, the best results were achieved with an Amberlyst catalyst but with lower conversion and selectivity values to h-GTBE than those obtained in a batch reactor.

The aim of this work was to explore the influence of the amount, strength and accessibility of Brønsted acid sites on the conversion and selectivity to h-GTBE for the catalytic etherification of glycerol with tert-butanol by modifying the acidic and porosity characteristics of three pentasil-type zeolites by different treatment procedures: protonation, dealumination, desilication-protonation, lanthanum exchange and fluorination.

2. Experimental

2.1. Catalysts preparation

Three commercial zeolites were modified by protonation, dealumination, desilication-protonation, lanthanum exchange and fluorination. Na-mordenite (Zeolyst, Si/Al = 6.5, CBV 10A Lot No. 1822-50), Na-Beta (Zeochem, Si/Al = 10, PB Lot No. 6000186) and Na-ZSM-5 (Zeochem, Si/Al = 20, PZ-2/40 Lot No. 6002827,01) were designated as M, B and Z, respectively.

Commercial zeolites were treated with NH_4NO_3 1 M at 373 K for 1 h. Samples were washed several times with deionised water and calcined at 813 K for 5 h to obtain the corresponding H-zeolites (HM, HB and HZ). Dealuminated zeolites were prepared from commercial Na-zeolites by refluxing with HCl 6 M at 373 K for 2 h (DAM, DAB and DAZ, respectively).

Samples DSHM, DSHB and DSHZ were obtained by desilication of commercial zeolites with NaOH 0.2 M under refluxing at 338 K for 30 min. After treatment, samples were washed until pH 7, dried, exchanged with NH_4NO_3 1 M at 373 K for 1 h and later calcined at 813 K for 5 h.

La-mordenite and La-beta were prepared by solid cation exchange adding $LaCl_3{\cdot}7H_2O$ (La/Al = 0.33) to 2 g of zeolite at 573 K for 3 h (samples LaM and LaB). After treatment, samples were filtered and washed several times with deionised water.

Finally, fluorinated mordenite, beta and ZSM-5 samples were obtained by adding 3.5 mL of NH_4F 0.1 M to 1 g of commercial zeolite to have 0.3 wt.% fluorine in the final sample. The slurry formed was stirred and kept at room temperature for 42 h. Lastly, samples were calcined at 723 K for 8 h (samples FHM, FHB and FHZ).

Two more beta samples were prepared combining fluorination and desilication treatments. Sample FHB was desilicated with NaOH 0.2 M by refluxing at 338 K for 30 min. After treatment, the sample was filtered, washed and dried overnight to obtain sample HB(F-DS). The other sample was prepared by desilication of commercial beta with NaOH 0.2 M by refluxing at 338 K for 30 min. Then, the sample was cation exchanged with NH_4NO_3 1 M at 373 K for 1 h, and later fluorinated at the same conditions as for preparing sample FHB, resulting in the sample HB(DS-F). Finally, sample FHB-zeolite A was prepared by physical mixing of sample FHB and commercial zeolite 4A (Sigma–Aldrich) in a weight ratio of 1/1.

One commercial Amberlyst-15 (sample A), supplied by Aldrich (39 m^2/g, pore size of 103 Å, pore volume of 0.34 cc/g, acidity of 4.7 meq H^+/g) was also used for comparison.

2.2. Catalysts characterization

Elemental analyses of the samples were obtained with a Philips PW-2400 sequential XRF analyser with Phillips Super Q software. All measures were made in triplicate.

Structural characterization was completed by powder X-ray diffraction patterns of the samples, which were obtained with a Siemens D5000 diffractometer using nickel-filtered Cu Kα radiation. Samples were dusted on double-sided sticky tape and mounted on glass microscope slides. The patterns were recorded over a range of 2θ angles from 5° to 40° and crystalline phases were identified using the Joint Committee on Powder Diffraction Standards (JCPDS) files (43-0171, 48-0074, 37-359 corresponds to mordenite, beta and ZSM-5, respectively). Crystallinity of the modified mordenites was determined by comparing the sum of the peak areas of (1 5 0), (2 0 2), (3 5 0) and (4 0 2) (22–32° 2θ) with respect to commercial Na-mordenite. Crystallinity of the modified ZSM-5 samples was calculated using the (0 5 1) peak intensity compared with the parent zeolite sample. The integrated intensity of the signal at $2\theta = 22.4°$ was used to evaluate the crystallinity of beta samples.

Textural characterization of the solids was performed by N_2 ($\sigma_{N2} = 0.162\ nm^2$) adsorption–desorption at 77 K using a Micromeritics ASAP 2000 surface analyser. Before measurements all samples were outgassed at 573 K for 6 h. BET surface areas were calculated using adsorption data in the relative pressure range $0 < P/P_0 < 0.1$. Micropore and external surface areas were obtained by t-plot analysis of the adsorption data in the $3.5 \leq t \leq 5$ Å t range by adopting the de Boer reference isotherm equation, whereas pore size distributions were determined by the Barrett–Joyner–Halenda (BJH) method.

Infrared spectra were recorded on a Bruker-Equinox-55 FTIR spectrometer. The spectra were acquired by accumulating 32 scans at 4 cm^{-1} resolution in the range of 400–4000 cm^{-1}. Samples were prepared by mixing the powdered solids with pressed KBr disks in a ratio of 5:95 and dried in an oven overnight. For adsorbed pyridine FTIR studies, samples were pressed into self-supported wafers, and activated at 623 K. Pyridine was adsorbed at 298 K, and infrared spectra were acquired by accumulating 64 scans at 4 cm^{-1} resolution in the range of 400–4000 cm^{-1}.

X-ray photoelectron spectra were taken with a SPECS system equipped with an Al anode XR50 source operating at 150 W and a Phoibos 150 MCD-9 detector with pass energy of 25 eV at 0.1 eV steps at a pressure below 6×10^{-9} mbar.

The acid content of commercial and modified zeolites was measured using established procedures employing thermal desorption of cyclohexylamine [26–28]. The method involves thermogravimetric analysis (TGA) following adsorption of the base on the catalysts and determines the number of acid sites capable of interacting with the base after heat treatment at 523 K. Samples were exposed to liquid cyclohexylamine at room temperature, after which they were kept overnight (at room temperature) and then in an oven at 353 K for 2 h so as to allow the base to permeate the samples [26–28]. The oven temperature was then raised to 523 K and maintained at that temperature for 2 h in order to remove all the physisorbed base. Cyclohexylamine desorption TGA curves were obtained using a Perkin Elmer TGA 7 microbalance equipped with a programmable temperature furnace. Each sample was heated from 323 to 973 K at heating rate of 10 K/min under nitrogen flow (25 mL/min). The weight loss associated with desorption of the base from acid sites was used to calculate the acid content in mmol of cyclohexylamine per gram of sample assuming that each mole of cyclohexylamine corresponds to one mole of protons [26–28].

^{1}H NMR and ^{27}Al NMR spectra were obtained with a Varian Mercury Vx 400 MHz with a probe of 7 mm CPMAS at a frequency of 400 MHz by spinning at 5 kHz. The pulse duration was 2 μs and the

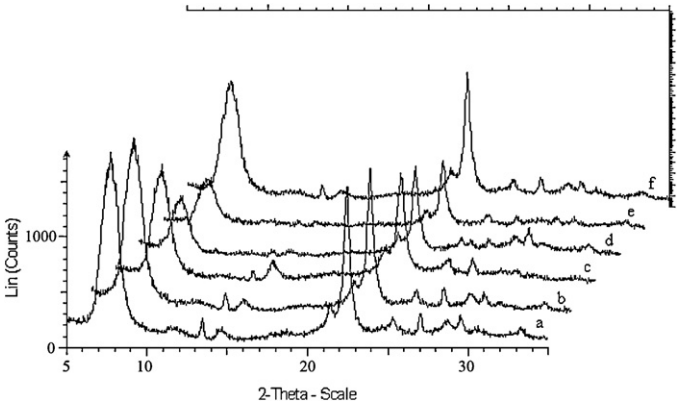

Fig. 1. XRD patterns for commercial and modified beta samples: (a) B, (b) HB, (c) DAB, (d) DSHB, (e) LaB, and (f) FHB.

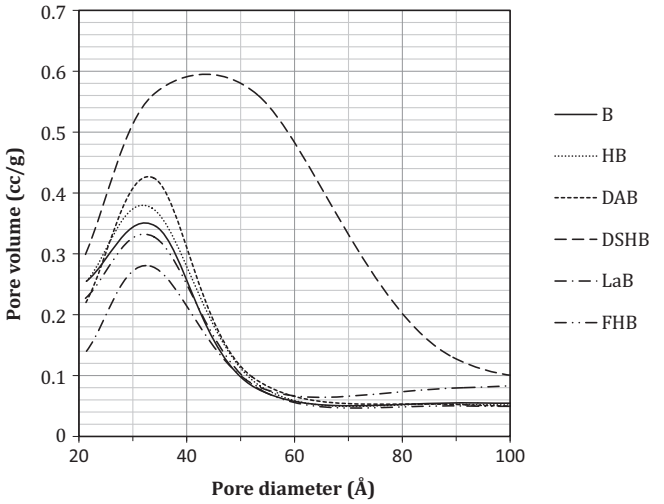

Fig. 2. Mesopore size distribution graphics for commercial and modified beta samples: (a) B, (b) HB, (c) DAB, (d) DSHB, (e) LaB, and (f) FHB.

delay time was 5 s. The chemical shift reference was trimethyl silil-3 propionic acid d_4-2,2,3,3 sodium salt for ^{1}H NMR, and high purity aluminium nitrate for ^{27}Al NMR.

2.3. Catalytic activity

Etherification experiments were performed in the liquid phase in a stainless steel stirred autoclave (150 mL) equipped with temperature controller and a pressure gauge. Stirring was fixed for all experiments at 1200 rpm to avoid external diffusion limitations. Typically, the composition of the reaction mixture was: 20 g of glycerol, glycerol/t-butanol molar ratio of 0.25, and constant catalyst loading of 5 wt.% (referred to glycerol mass). Catalysts were dried before testing. The reaction temperature used was 348 K. Some experiments were performed at 363 K, or with a glycerol/t-butanol molar ratio of 0.125. Samples were usually taken at 1, 3, 6 and 24 h of reaction. The reaction products were analysed by gas chromatography using a chromatograph model Shimadzu GC-2010 equipped with a SupraWax-280 column and a FID detector.

Glycerol conversion and selectivity to MTBG (glycerol monoethers) were determined from calibration lines obtained from commercial products. For DTBG (glycerol diethers) and TTBG (glycerol triether), which were not available commercially, we isolated them from the products of the etherification reaction by column chromatography (1:9 ethyl acetate/hexane) and identified them by ^{13}C and ^{1}H NMR for proper quantification with the assistance of the characterization data reported by Jamróz et al. [29].

3. Results and discussion

3.1. Catalysts characterization

H-zeolites (HM, HZ and HB) maintained the zeolite structure (see Fig. 1a and b) showing similar crystallinity than their corresponding Na-zeolites (Table 1). HM, HZ and HB had slightly higher Si/Al ratio than M, Z and B, respectively. Additionally, we observed a shift to higher frequency values of the IR bands assigned to symmetric and asymmetric stretching of the T—O bond (T = Si, Al) for these protonated samples (Table 1). The increase of the strength of the T—O bond can be related to a decrease in the Al content since the Si—O bond is shorter than the Al—O bond, and Al has lower electronegativity than Si [30]. These results indicate that some dealumination occurred for H-zeolites due to the temperature used during calcination, as reported by other authors [31]. This agrees with the slight higher mesoporosity and slight higher surface areas observed for protonated samples (e.g. Fig. 2, Table 1). The acidity of H-zeolites was higher than that of Na-zeolites (Table 1), as expected, due to the presence of H^+ compensating the negative charge of the zeolite framework. ^{1}H NMR spectra of commercial zeolites showed one peak around 4 ppm (e.g. Fig. 3a), which can be attributed to free Brønsted protons [32,33]. After protonation, this peak, related to the protons formed during the treatment, shifted to higher ppm values (Table 1, e.g. Fig. 3b), as expected [34].

We observed dealumination for all the acid-treated zeolites (DAM, DAZ and DAB) since they showed higher Si/Al ratio, lower cell values, and a shift to higher frequencies of the IR bands assigned to symmetric and asymmetric stretching of the T—O bond (T = Si, Al) than their corresponding Na-zeolites (Table 1). The extent of dealumination was function of the zeolite structure. Thus, beta zeolite was easier to dealuminate than mordenite, whereas dealumination of ZSM-5 was very low. This order can be related to the flexibility of each zeolite framework, and the accessibility of the aluminium atoms depending on the pores arrangement and sizes [31,33]. Mordenite and ZSM-5 zeolites are less flexible than beta, and consequently, it is more difficult to dealuminate them. Additionally, zeolite beta crystallizes with many stacking faults [35] while mordenite samples, although less frequently, may also have structurally related stacking faults [36]. Stacking faults increase the probability of the presence of defect sites in the framework. Also, the number of the T-atoms in four-rings may have an influence on the stability towards dealumination because the tension in the smaller rings is larger. Thus, a zeolite is easier to dealuminate as many aluminium atoms has in an environment with tension [31]. The acid and heating conditions used here did not cause drastic changes in the zeolite structures (e.g. Fig. 1c), although there was some decrease in the crystallinity of mordenite and beta zeolites after acid treatment (Table 1). The crystallinity of ZSM-5 samples practically did not change as a result of their low dealumination. From nitrogen physisorption results, acid-treated mordenite and acid-treated ZSM-5 presented higher surface area and lower micropore area/external surface area ratios. This tendency appeared more marked for the mordenite sample. This can be attributed to the loss of aluminium in the zeolite structure, which results in higher mesoporosity, and therefore, higher surface area. However, after dealumination of beta zeolite, we observed a decrease in the BET surface area despite the slight higher mesoporosity obtained (Fig. 2). This can be associated with the loss of crystallinity observed after treatment, as reported by other authors [37]. Partially dealuminated samples showed lower amounts of Brønsted acidity than their starting zeolites (Table 1), as expected, due to the loss of

Table 1
Characterization of commercial and modified zeolites by XRF, XRD, N_2 physisorption, FTIR, TGA and ^{1}H NMR techniques.

Catalyst	Si/Al (XRF)	Crystallinity[a] (%)	Unit cell volume[a] (Å^3)	BET area[b] (m^2/g)	External surface area[b] (m^2/g)	Micropore area/External surface area[b]	IR bands (cm^{-1})[c]		Acidity capacity (mmol H$^+$/g)	^{1}H NMR (ppm)
							ν_1	ν_2		
M	6.5	100	2791	303	31	8.9	1068	629	0.10	4.6
HM	6.9	93	2790	312	43	7.1	1075	630	0.18	6.1
DAM	18.2	75	2747	412	54	5.1	1093	646	0.08	5.1
DSHM	4.7	62	2776	319	45	6.0	1075	636	0.15	4.4
LaM	6.5	67	2793	149	22	1.6	1069	627	0.16	6.4
FHM	7.0	88	2784	304	34	8.1	1070	628	0.11	6.5
B	10.0	100	–	573	203	1.8	1068	629	0.41	4.2
HB	11.0	89	–	579	218	1.7	1086	633	0.60	4.4
DAB	110.7	61	–	554	197	1.5	1091	641	0.18	4.0
DSHB	4.2	56	–	663	304	1.2	1078	630	0.50	3.9
LaB	10.1	44	–	384	133	1.5	1068	628	0.55	4.5
FHB	11.8	82	–	496	142	1.7	1073	629	0.46	4.7
Z	20.0	100	5209	300	87	2.4	1063	797	0.25	3.8
HZ	20.2	100	5186	307	114	2.3	1068	797	0.37	4.2
DAZ	22.3	99	5172	334	127	2.1	1096	797	0.21	4.0
DSHZ	14.2	97	5122	353	135	1.6	1073	795	0.28	3.7
FHZ	20.3	100	5154	305	110	1.8	1065	797	0.26	4.8

[a] Calculated from XRD patterns.
[b] Calculated from N_2 physisorption results.
[c] Frequencies of the main asymmetric stretch (ν_1), and the main symmetric stretch (ν_2) due to the T—O bond (T = Si, Al).

extraframework cations as a consequence of the dealumination. ^{1}H NMR spectra of DAM and DAZ presented one broad peak at higher ppm values than that observed for M and Z, respectively (Table 1). This peak could be assigned to Brønsted protons, formed by cation exchange during dealumination in HCl medium, which are interacting with the zeolite framework [31,33]. For DAB, we observed one peak in the ^{1}H NMR spectrum (Fig. 3c) with a shift similar to that of commercial beta (Fig. 3a). This can be explained by the higher dealumination suffered by this sample. Therefore, there are no protons interacting with the framework since practically the zeolite framework has no negative charge.

All basic-treated and later protonated samples (DSHM, DSHB, DSHZ) showed desilication since they had lower Si/Al ratios and lower cell volume values than commercial zeolites (Table 1). The frequencies of the IR bands assigned to symmetric and asymmetric stretching of the T—O bond (T = Si, Al) had similar values (Table 1) to those reported by other authors for desilicated zeolites [38]. Additionally, some dealumination cannot be discarded due to the temperature used during calcination in the last step of protonation. Desilication was higher for beta than for ZSM-5 and mordenite. This can be related to the low stability of framework aluminium in beta compared to ZSM-5 and mordenite taking into account that lattice aluminium controls silicon extraction of the zeolite framework [39]. The zeolite structure maintained after desilication-protonation treatment (e.g. Fig. 1d), although some decrease in the crystallinity of mordenite and beta was observed (Table 1). Desilicated-protonated samples showed higher surface area and higher mesoporosity (e.g. Fig. 2) than their corresponding starting zeolites, as expected, due to the loss of silicon in the zeolite structure. Interestingly, acidity was slightly higher (Table 1) but the peak observed in the ^{1}H NMR spectrum shifted to lower ppm values (Table 1, e.g. Fig. 3d) for the desilicated samples than for the commercial ones. The slight higher acidity can be explained by the second step of protonation applied to desilicated samples that led to the presence of H$^+$ in these modified zeolites whereas the less strength of these acid sites could be related to variations in the zeolite composition due to the treatment.

La-containing samples exhibited similar Si/Al ratio than their corresponding commercial zeolites (Table 1). This agrees with the similar frequencies values of the IR bands assigned to symmetric and asymmetric stretching of the T—O bond (T = Si, Al) obtained for these samples (Table 1). XRD patterns of LaB and LaM showed the maintenance of the zeolite structure (e.g. Fig. 1e) although a considerable decrease of crystallinity was observed for both samples (Table 1). The lower surface areas accompanied by some decrease of porosity (e.g. Fig. 2) observed for La-modified samples can be attributed to the presence of bulky hydrolysed lanthanum cations ($La(OH)_2^+$) blocking the pores. The introduced hydrolysed lanthanum cations led to similar amount of acid sites than their corresponding H-zeolites (Table 1) but with slightly stronger Brønsted acidity (a shift to higher ppm values was observed in the ^{1}H NMR spectra, e.g. Fig. 3e) according to the results reported by other authors [40,41]. The lanthanum exchanged in the zeolites can cause a polarization of the zeolite framework increasing the strength of the Brønsted acid sites [42].

Zeolite modification by treatment with NH_4F practically did not affect the zeolite structure (e.g. Fig. 1f), except for some decrease in the crystallinity detected for FHM and FHB (Table 1). In addition, the Si/Al ratio, the position for the symmetric and asymmetric TO_4 tetrahedra bands in the mid-IR region (Table 1) and the nitrogen adsorption–desorption isotherm shapes of the fluorinated samples were very similar to those observed for their corresponding Na-zeolites (Table 1, e.g. Fig. 2). The presence of fluorine in the zeolite framework was confirmed by XPS. F1s XP spectra of fluorinated samples showed one peak with two components: one at ca. 685 with much higher area than the other appeared at ca. 687 eV (e.g. Fig. 5). These two peak components can be assigned to fluoride species interacting with Al atoms, and with Si atoms, respectively (Scheme 1) according to the results reported by other authors for fluorinated zeolites [43]. The formation of fluorocomplexes of Al by the introduction of fluorine in the zeolite framework has been related to an increase in the acidity of the Brønsted acid sites through an inductive effect by fluorine whereas the formation of fluorocomplexes of Si has been correlated with a decrease of the Brønsted/Lewis acidity ratio [43]. Therefore, the higher contribution of the component appeared at 685 eV observed for our fluorinated samples indicated the incorporation of fluorine in the zeolite framework. ^{27}Al NMR spectra of fluorinated samples were very similar to those of the starting zeolites (e.g. Fig. 4). This indicates that fluorination at mild conditions did not cause appreciable dealumination. The signals corresponding to tetrahedral and octahedral aluminium appear around 50 ppm and 0 ppm, respectively. The

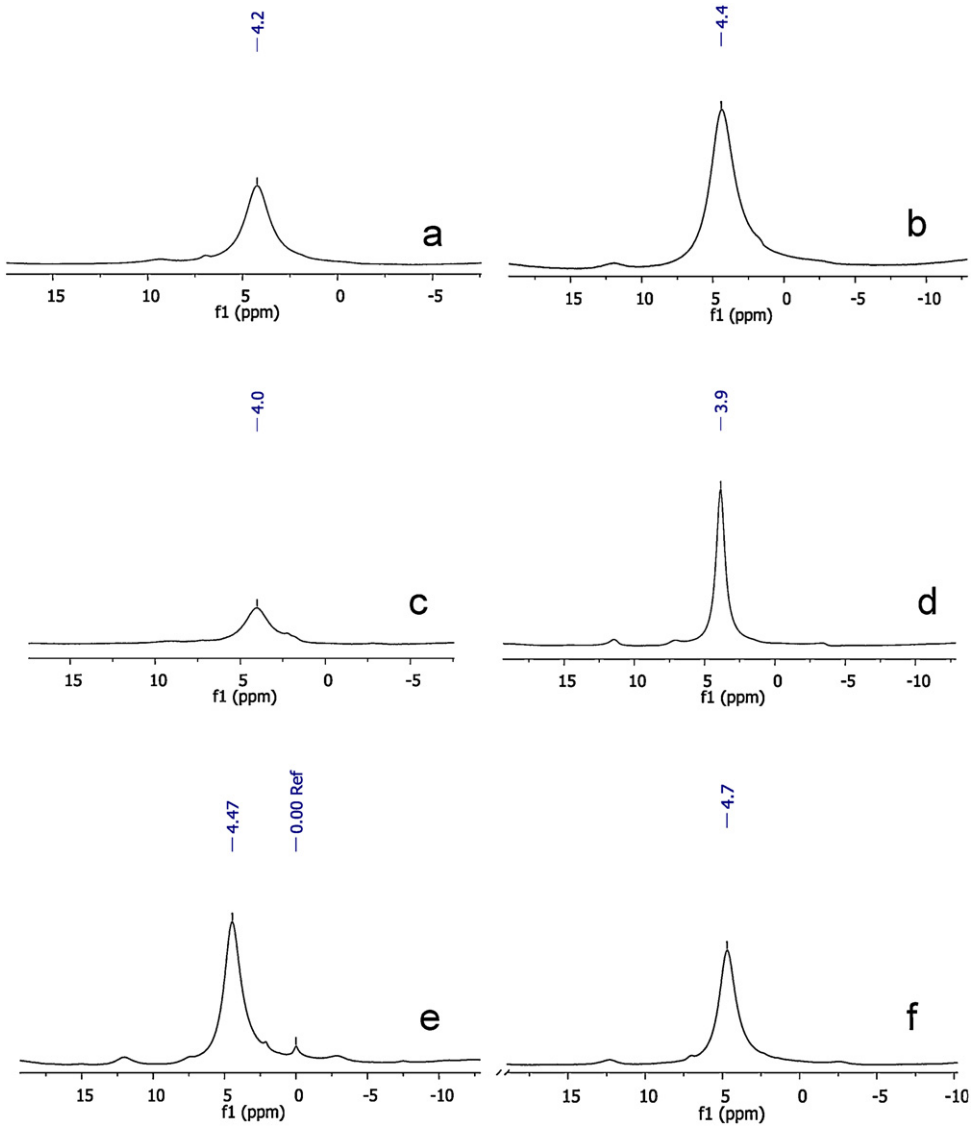

Fig. 3. ^{1}H NMR spectra of the samples (a) B, (b) HB, (c) DAB, (d) DSHB, (e) LaB, and (f) FHB.

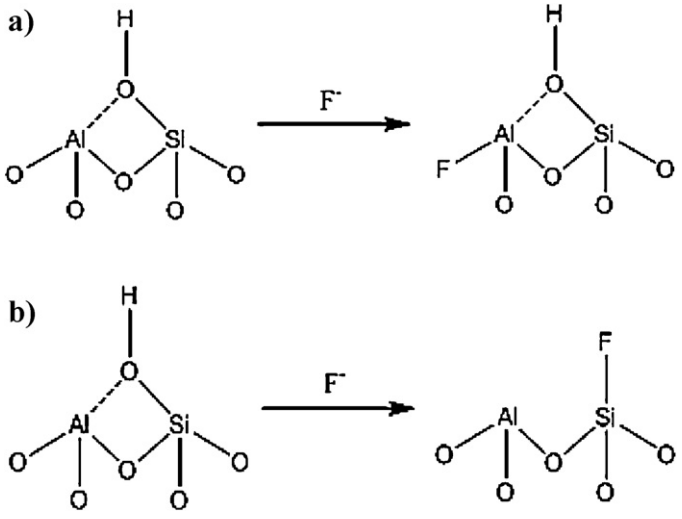

Scheme 1. Fluorination mechanism of zeolites: (a) formation of fluoride species interacting with Al atoms, and (b) formation of fluoride species interacting with Si atoms.

presence of octahedral Al in commercial beta can be attributed to extraframework aluminium species or to aluminium coordinated in defect sites taking into account the characteristic stacking faults of this zeolite structure [35,44]. Acidity capacity values of fluorinated samples were slightly higher than those of Na-zeolites (Table 1). Additionally, from ^{1}H NMR results, we observed that, after fluorination, the peak attributed to Brønsted protons that are interacting with the zeolite framework, shifted to higher ppm values (e.g. Fig. 3f). This only can be explained by an inductive effect by F confirming the introduction of fluorine atoms in the zeolite framework.

3.2. Catalytic activity

Table 2 shows the catalytic activity results obtained for all zeolite catalysts for the etherification reaction of glycerol with tert-butanol after 24 h of reaction. One acid ion-exchange resin (Amberlyst 15, here named as A), which is a typical acid catalyst used for this reaction, has been also tested at the same reaction conditions for comparison. The reaction products obtained were mono-tert-butyl glycerol ether (MTBG), di-tert-butyl glycerol ether (DTBG) and sometimes low amounts of tri-tert-butyl glycerol ether (TTBG). No other reaction products were detected in any case.

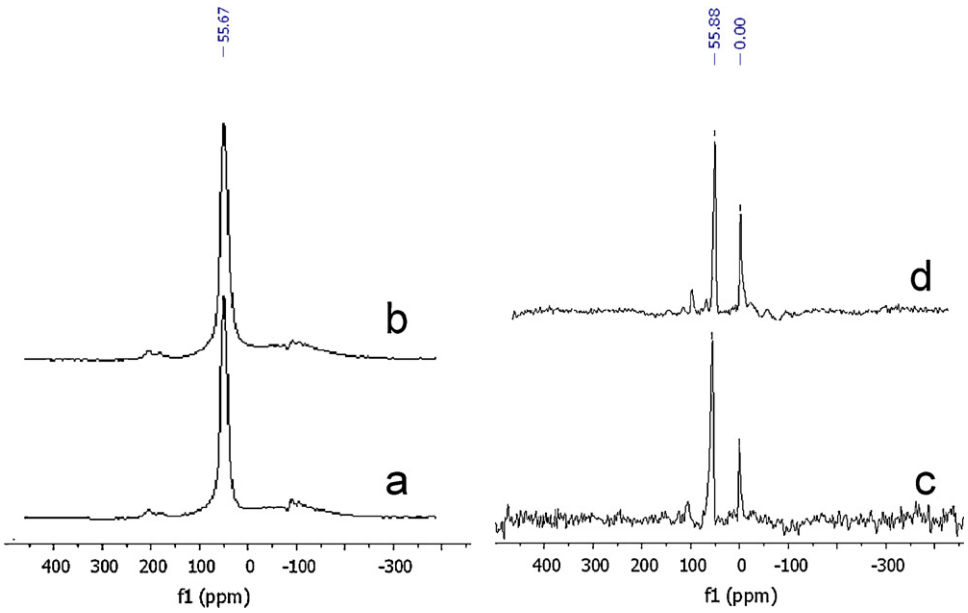

Fig. 4. ^{27}Al MAS NMR for (a) NaM, (b) FHM, (c) NaB, and (d) FHB samples.

On the whole, independently on the modifications performed, beta catalysts were more active than ZSM-5 and mordenite catalysts in this order (Table 2). This behaviour was previously observed, specifically when the same commercial Na-zeolites used in this study were tested for the isomerization of styrene oxide to β-phenylacetaldehyde, a reaction catalysed by Brønsted acid sites [33]. The differences in the activity between the catalysts prepared from the three types of zeolites could be explained by the number of Brønsted acid sites and their strength (Table 1) together with the accessibility of the reactants to the active sites. Beta and ZSM-5 samples had much higher external surface area and higher acid capacity than mordenite samples (Table 1) despite to have a three-dimensional pore structure compared with the one-dimensional pore structure of mordenite. Thus, zeolite beta has a three-dimensional 12-ring pore system (straight channels of diameter 6.6 Å × 6.7 Å and sinusoidal channels of diameter 5.6 Å × 5.6 Å), zeolite mordenite has a one-dimensional pore system with main channels of diameter 6.7 Å × 7.0 Å and compressed channels of diameter 2.6 Å × 5.7 Å whereas ZSM-5 has a three-dimensional 10-ring pore system with channels of diameter 5.1 Å × 5.5 Å. Additionally, it is important to note that mordenite is the most hydrophilic structure of the three zeolites used in this study since it has the lowest Si/Al ratio (Table 1). Taking into account that water is formed during reaction, a major competition between water and the reactants for the active sites can be expected for this zeolite. All these factors could explain the lower conversion values obtained for mordenite catalysts.

Table 2
Catalytic activity of Amberlyst-15, commercial and modified mordenite, beta and ZSM-5 catalysts.

Catalyst	Conversion (%)	MTBG (%)	h-GTBE (%)
A	81	64	36 (1)
M	10	77	23
HM	29	89	11
HM[a]	30	78	22
DAM	27	100	0
DSHM	8	95	5
LaM	23	100	0
FHM	32	81	9
B	63	74	26
B[b]	83	74	26
HB	66	66	34
HB[c]	71	70	30
DAB	29	100	0
DSHB	61	82	18
LaB	16	78	22
FHB	75	63	37 (1)
Z	35	100	0
HZ	58	96	4
DAZ	22	100	0
DSHZ	22	97	3
FHZ	33	92	8

Reaction conditions: 5.0 wt.% of catalyst referred to glycerol mass, glycerol/t-butanol molar ratio = 0.25, reaction temperature = 348 K, reaction time = 24 h, stirring = 1200 rpm. MTBG: glycerol monoethers; h-GTBE: glycerol diethers + glycerol triether. In parenthesis, selectivity to glycerol triether (%).

[a] Reaction time = 48 h.

[b] Glycerol/t-butanol molar ratio = 0.125.

[c] Glycerol/t-butanol molar ratio = 0.125 and reaction temperature = 363 K.

Regarding the catalytic results of Beta samples (Table 2), we can observe that Na-Beta showed lower conversion and lower selectivity to high-glycerol tert-butyl ethers (h-GTBE) than Amberlyst-15 (catalyst A). This can be related to the lower amount and strength of acid sites of Na-Beta compared with Amberlyst-15, a macroporous acid ion-exchange resin with sulfonic groups. The activity of commercial Na-zeolites can be attributed to the presence of free Brønsted protons, as detected by ^{1}H NMR [32,33]. When B was

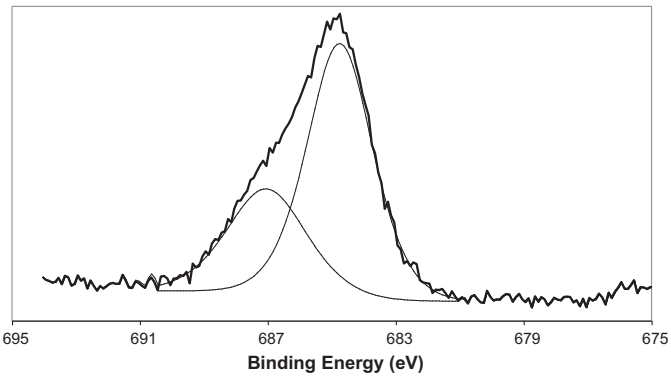

Fig. 5. Deconvoluted F 1 s XP spectrum of the sample FHB.

tested at lower glycerol/t-butanol ratio, conversion increased and was comparable to that of Amberlyst-15 but the products selectivity values did not change (Table 2). H-Beta led higher conversion and higher selectivity to h-GTBE than Na-Beta, as expected, taking into account the higher amount and strength of its Brønsted acid sites (Table 1). When HB catalyst was tested at higher reaction temperature (363 K) and lower glycerol/t-butanol ratio, conversion increased but again the selectivity to h-GTBE did not improve (Table 2). One important feature to remark is that triether was not detected for Na-Beta or H-Beta. This has been attributed by other authors to steric hindrance effects because of the microporosity of the zeolites [14]. Partially dealuminated beta (DAB) presented lower conversion than its corresponding Na- and H-beta, and null selectivity to h-GTBE (Table 2). This can be related to the lower amount of acid centres, which also had slight lower acidity, observed for DAB due to dealumination (Table 1). This reveals the importance of acidity for this reaction since the additional mesoporosity generated during dealumination was not enough to favour the formation of the high-glycerol tert-butyl ethers (di- and triether). Desilicated-protonated Beta (DSHB) also showed lower conversion and lower selectivity to h-GTBE than B or HB (Table 2). This was surprising since this catalyst had slight higher acidity capacity and higher mesoporosity to avoid possible steric hindrance than those previously discussed (Table 1). These results can be explained by the lower strength of the Brønsted acid sites of desilicated samples, as observed from ^{1}H NMR (Table 1). Therefore, the acid strength of the catalytic sites influences significantly the catalytic performance, both conversion and selectivity to h-GTBE. La-containing beta catalyst showed the lowest conversion of all beta catalysts without improving the selectivity to h-GTBE (Table 2). The presence of bulky hydrolysed lanthanum cations ($La(OH)_2^+$) blocking the pores increased steric hindrances despite the higher strength of the Brønsted acid sites of this catalyst (Table 1). Thus, the accessibility of the reagents to the catalytic sites strongly affects the catalytic results. Finally, fluorination of beta zeolite at mild conditions resulted in a catalyst, which yielded the best conversion and selectivity to h-GTBE due to the higher amounts of the strongest Brønsted acid sites generated because of the incorporation of fluorine in the zeolite framework. Interestingly, FHB allowed us to detect the presence of tri-tert-butyl glycerol ether (TTBG) in low amounts. This is the first time that the formation of glycerol triether in a zeolite, for the glycerol etherification with tert-butanol, has been reported. Taking into account that this catalyst has similar porosity than NaB or HB (Table 1 and Fig. 2), we can conclude that the higher acidity strength achieved by incorporating low amounts of fluorine in the zeolite structure is fundamental to favour the production of the bulky triether. Additionally, catalytic activity of this catalyst was comparable to that obtained with Amberlyst-15 (Table 2).

All ZSM-5 catalysts showed moderate conversion values and very low or null selectivity to h-GTBE (Table 2). From these catalytic results, we can conclude that the modifications made on this zeolite by the different treatments did not affect considerably its surface and acidic properties (Table 1) and, consequently, its catalytic behaviour. The most interesting result is that fluorination of ZSM-5 at mild conditions, allowed to obtain a catalyst (FHZ), which led to slight higher selectivity to h-GTBE than the rest of ZSM-5 catalysts. This only can be related to the generation of stronger Brønsted acid sites (Table 1), as previously observed for fluorinated beta catalyst, because of the incorporation of fluorine in the zeolite framework.

Mordenite catalysts showed a catalytic behaviour very different when compared with ZSM-5 and beta catalysts. Commercial Na-mordenite showed low conversion but comparable selectivity to h-GTBE than commercial Na-beta (Table 2). The lower conversion could be related to the lower amount of acid centres, lower external surface area, more hydrophilic character and lower dimensionality of the mordenite structure, as previously commented, whereas the selectivity to h-GTBE could be attributed to its higher acidity strength (Table 1). After protonation, conversion increased, as expected due to the presence of higher amounts of acid centres with higher acidity strength but the selectivity to h-GTBE was lower (Table 2). This tendency was also observed for the partially dealuminated mordenite (DAM) and for fluorinated mordenite (FHM). These catalysts had similar amount of acid sites but with stronger acidity than Na-mordenite (Table 1). The low external surface area and the lower dimensionality and higher hydrophilic character of the mordenite structure could affect the subsequent consecutive reactions from the higher amounts of monoether formed initially on these most active mordenite catalysts. Probably, longer reaction times should be required to favour the equilibrium for the formation of di- and triethers. Actually, when HM was tested for 48 h of reaction, higher selectivity to h-GTBE was achieved (Table 2). Desilicated-protonated mordenite showed lower conversion and lower selectivity to h-GTBE than Na-mordenite. This can be explained by the slight lower acidity strength of its acid sites. The incorporation of lanthanum in mordenite did not improve the conversion values obtained with HM or DAM and yielded total selectivity to the undesired glycerol monoethers (Table 2). This catalytic behaviour was previously observed for LaB. The presence of bulky hydrolysed lanthanum cations ($La(OH)_2^+$) blocking the pores increased steric hindrances despite the higher strength of the Brønsted acid sites of this catalyst (Table 1).

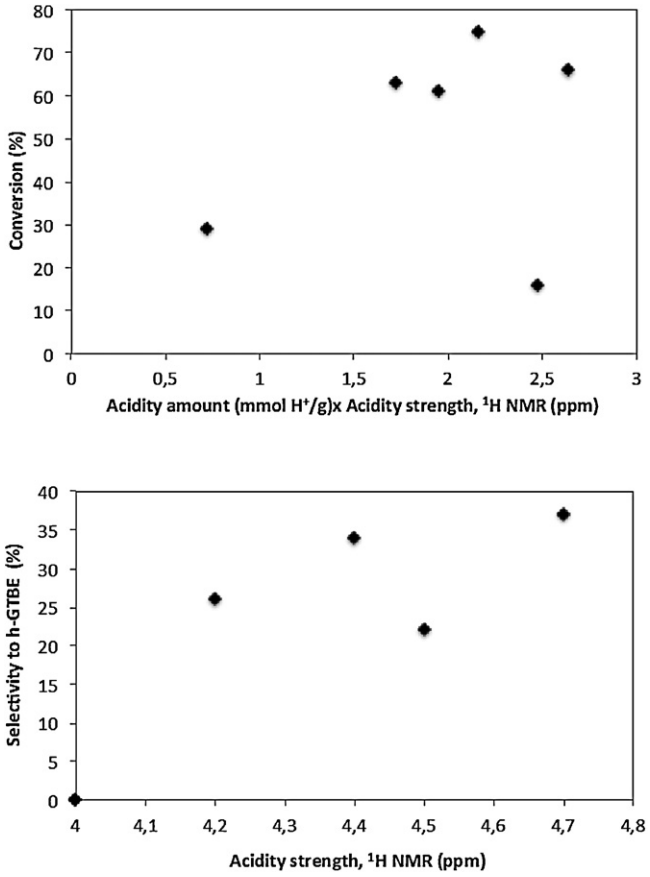

Fig. 6. Conversion vs acidity amount × acidity strength, and selectivity to h-GTBE vs acidity strength graphs for beta catalysts. Reaction conditions: 5.0 wt.% of catalyst referred to glycerol mass, glycerol/t-butanol molar ratio = 0.25, reaction temperature = 348 K, stirring = 1200 rpm.

Fig. 6 represents conversion vs acidity amount × acidity strength, and selectivity to h-GTBE vs acidity strength for beta

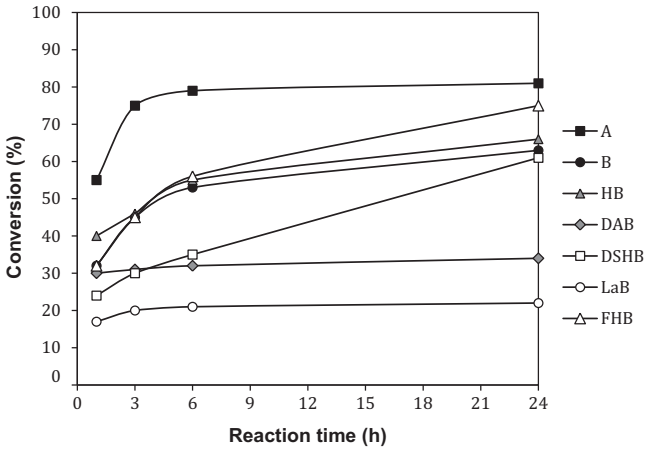

Fig. 7. Study of the variation of conversion with time for beta catalysts. Reaction conditions: 5.0 wt.% of catalyst referred to glycerol mass, glycerol/t-butanol molar ratio = 0.25, reaction temperature = 348 K, stirring = 1200 rpm.

catalysts. As we can observe, there is quite good lineal correlation between conversion with respect to acidity amount × acidity strength, except for one of the points which corresponds to the LaB sample. This confirms that the amount and strength of Brønsted acid sites strongly influences conversion values. For LaB sample, the presence of bulky hydrolysed lanthanum cations ($La(OH)_2^+$) blocking the pores increased steric hindrances despite the higher strength of the Brønsted acid sites of this catalyst, as commented above. Interestingly, selectivity to h-GTBE vs acidity strength also showed good correlation, indicating that acidity strength mainly affects selectivity to di- and tri-ethers. For mordenite and ZSM-5 samples, representation of conversion vs acidity strength × acidity amount and selectivity to h-GTBE vs acidity strength (not shown here) did not exhibit clear correlations in any case. This means, that other factors, such as the accessibility or diffusion of the reactants to the acid sites, also influences conversion and selectivity values for these catalysts.

Fig. 7 shows the variation of conversion with time for Amberlyst and beta-zeolite catalysts. Conversion of Amberlyst increased from 1 to 6 h of reaction, but after this time, maintained practically constant. In contrast, for NaB, HB, DSHB and FHB catalysts the increase of conversion with time was more gradual and continuous even after 6 h of reaction. Lastly, conversion values of catalysts DAB and LaB practically did not change with the reaction time. The variation of activity with time of these catalysts was accompanied by a decrease of their surface areas (Table 3) and a considerably decrease of their Brønsted acid sites (e.g. Fig. 8). This indicates a loss of active centres during reaction, and therefore some catalysts deactivation. However, XRD did not show significant changes in the zeolite structure after reaction in any case except for some decrease in crystallinity (e.g. Fig. 9). From these results, we can conclude that there is no collapse of the structure during reaction, but blocking of pores by reaction products. One of the problems of this reaction

Table 3
Characterization of several beta-zeolite catalysts before reaction, after 24 h of reaction, and after extraction.

Catalyst	BET area before reaction (m^2/g)	BET area after reaction (m^2/g)	BET area after extraction (m^2/g)
B	573	361	457
HB	579	364	429
DAB	554	99	387
DSHB	663	124	498
LaB	384	45	276
FHB	496	334	470

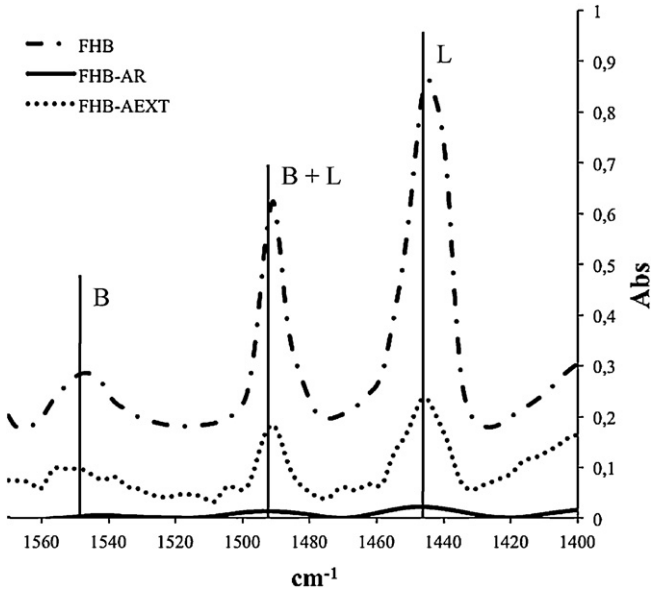

Fig. 8. FTIR spectra of adsorbed pyridine for FHB, FHB-AR (after reaction) and FHB-AEXT (after extraction). B: Brønsted acid sites; L: Lewis acid sites.

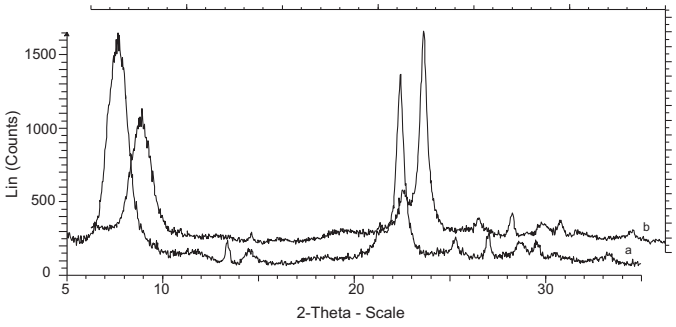

Fig. 9. XRD patterns of catalyst FHB: (a) before reaction and (b) after reaction.

is that the formation of water during reaction inhibits the glycerol etherification since water competes with tert-butanol and glycerol for the active site adsorption [24]. The more gradual variation of conversion with time observed for NaB, HB, DSHB and FHB with respect to the acid ion-exchange resin can be related to the nature of the zeolite, which can partially adsorb the water formed during reaction in contrast with Amberlyst, which was strongly affected by the presence of water, as reported by other authors [24]. The almost no variation of conversion observed for DAB and LaB catalysts can be explained by the low amount of acid centres of catalyst DAB, and because of the effect of bulky $La(OH)_2^+$ cations blocking the pores for LaB.

Table 4
Catalytic activity of beta catalysts after 6 h of reaction.

Catalyst	Conversion (%)	MTBG (%)	h-GTBE (%)
B	53	73	27
HB	55	70	30
DAB	32	100	0
DSHB	35	82	18
LaB	21	80	20
FHB	56	77	23

Reaction conditions: 5.0 wt.% of catalyst referred to glycerol mass, glycerol/t-butanol molar ratio = 0.25, reaction temperature = 348 K, reaction time = 6 h, stirring = 1200 rpm. MTBG: glycerol monoethers; h-GTBE: glycerol diethers + glycerol triether. In parenthesis, selectivity to glycerol triether (%).

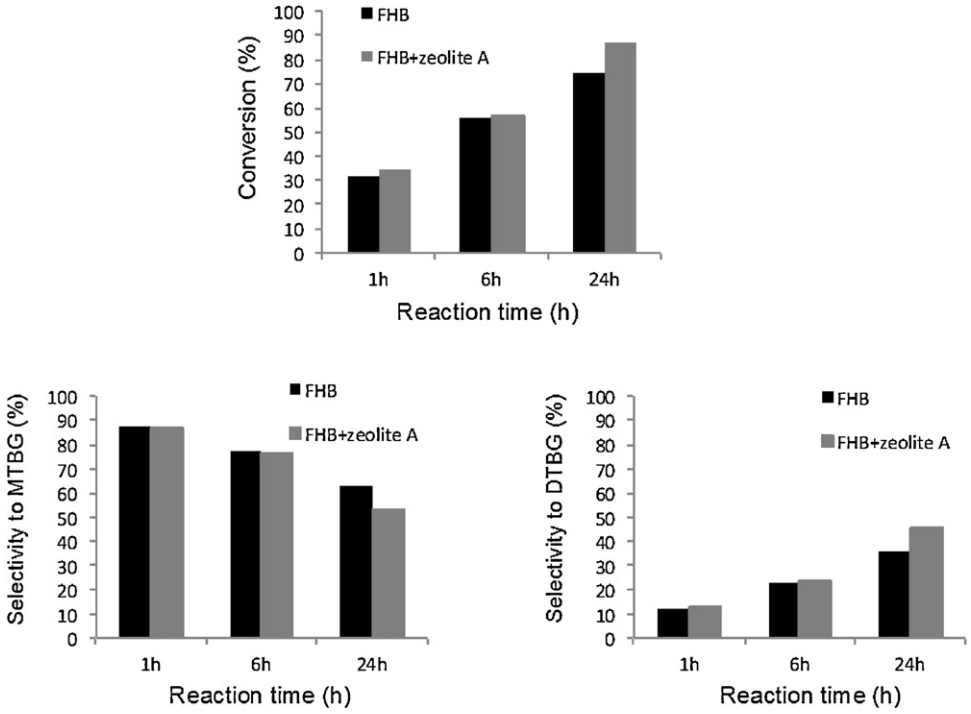

Fig. 10. Comparison of conversion and selectivity to the three-glycerol ethers with the reaction time for catalysts FHB and FHB mixed with zeolite A. Reaction conditions: 5.0 wt.% of catalyst referred to glycerol mass, glycerol/t-butanol molar ratio = 0.25, reaction temperature = 348 K, reaction time = 24 h, stirring = 1200 rpm. MTBG: glycerol monoethers; DTBG: glycerol diethers.

Regarding selectivity values, Table 4 shows the results obtained for beta catalysts after 6 h of reaction. On the whole, at lower reaction times selectivity to h-GTBE was similar or slight lower than after 24 h of reaction. Therefore, higher reaction times favoured slightly the obtention of higher amounts of h-GTBE. Interestingly, glycerol triether was not observed for catalyst FHB at lower reaction times, even after 12 h or 18 h of reaction (not shown here).

In order to evaluate the nature of the products remaining in the catalytic pores after reaction, several used catalysts, after filtration, were submitted to extraction by refluxing with 50 mL of ethanol for 1 h. After rotary evaporation of the solvent, the resulting solution was analysed by gas chromatography. All chromatograms showed the presence of several peaks corresponding to glycerol and products of reaction (monoethers and diethers in less proportion). Interestingly, surface areas and the amount of Brønsted acid sites of the catalysts were partially recovered after extraction (Table 3, e.g. Fig. 8). Therefore, the presence of reagents and reaction products in the pores decreases the accessibility of the reagents to the acid sites.

From all these results, we tried to improve the selectivity towards the triether detected with FHB. Thus, four new fluorinated beta catalysts were synthesized at different conditions and tested for this reaction. Two samples were prepared by the same method as FHB but increasing the theoretical fluorine content to obtain 1 wt.% F (FHB(1%)) and 10 wt.% F (FHB(10%)), with the idea to increase the number of stronger acid sites. The other two samples were synthesized by combining desilication and fluorination procedures (HB(DS-F) and HB(F-DS)), as described in Section 2, with the aim to increase acidity and mesoporosity at the same time. The catalytic results of these four new catalysts are shown in Table 5.

As we can observe, the increase in the percentage of theoretical fluorine did not improve the catalytic results obtained for sample FHB. This suggests that not all the theoretical fluorine was introduced in the zeolite structure and some framework dealumination occurred for both samples (especially for FHB(10%)). Dealumination was confirmed (not shown here) by the decrease of the cell volumes, the gradual increase of octahedral aluminium observed by ^{27}Al NMR, the higher mesoporosity and the shift to higher frequencies of the IR bands, assigned to symmetric and asymmetric stretching of the T—O bond (T = Si, Al) of these two samples when comparing with the starting zeolite. Therefore, fluorination treatment with higher amounts of fluorine did not increase significantly the introduction of fluorine in the structure, and for this reason, the catalytic results of these catalysts were very similar to those of FHB.

Si/Al ratios, determined by XRF, were 4.0 and 4.1 for HB(DS-F) and HB(F-DS), respectively, confirming desilication. The sample first desilicated and later fluorinated had less wt.% fluorine (0.1) than the sample first fluorinated and later desilicated (0.25) as determined by chemical analysis. This explains the catalytic results obtained since catalyst HB(DS-F) showed lower conversion and lower selectivity to h-GTBE whereas catalyst HB(F-DS) had similar conversion and slight lower selectivity to h-GTBE than FHB (Table 2). Interestingly, low amounts of tri-tert-butyl glycerol ether (TTBG) were detected for all four catalysts. This confirms the influence of the introduction of fluorine in the zeolite structure on the acidity, and therefore, the significant effect of the stronger Brønsted acidity, generated by fluorination, on the formation of the triether, independently of the porosity.

Table 5
Catalytic activity results of several fluorinated beta catalysts for the glycerol etherification with tert-butanol.

Catalyst	Conversion (%)	MTBG (%)	h-GTBE (%)
FHB(1%)	72	64	36 (1)
FHB(10%)	70	66	34 (1)
HB(DS-F)	51	90	10 (<1)
HB(F-DS)	74	70	30 (1)

Reaction conditions: 5.0 wt.% of catalyst referred to glycerol mass, glycerol/t-butanol molar ratio = 0.25, reaction temperature = 348 K, reaction time = 24 h, stirring = 1200 rpm. MTBG: glycerol monoethers; h-GTBE: glycerol diethers + glycerol triether. In parenthesis, selectivity to glycerol triether (%).

As commented above, one of the problems of this reaction is the formation of water during reaction [24]. The higher water acidity in relation to tert-butanol results in a lowering of catalyst activity due to the formation of solvated sites, as reported in the literature [45,46]. Frusteri et al. proposed that the removal of water from the reaction medium could increase the formation of high glycerol ethers [24]. These authors performed one experiment by stopping the etherification reaction after 6 h, dehydrated the reaction mixture by zeolites, and then continued with the reaction for 6 more hours. The results showed an important increase in the formation of diethers [24]. From this idea, we designed one similar catalytic experiment using a mixture of sample FHB and commercial zeolite 4A in a weight ratio of 1/1 as catalyst. Zeolite A was inactive for this reaction. Fig. 10 shows the comparative evolution with time of conversion and selectivity towards the three-glycerol ethers for catalysts FHB and FHB-zeolite A. After 1 h of reaction, the catalytic results were just slightly better for the catalyst mixed with the molecular sieve. This improvement in the conversion and selectivity to h-GTBE were more marked at higher reaction times. This confirms that the presence of zeolite A in the medium helped to adsorb the water generated during the etherification reaction allowing a better approach of the reagent molecules to the Brønsted acid sites of catalyst FHB, and therefore favouring the formation of high ethers. We also observed a higher slight increase of the triether amount with time for the catalyst mixed with zeolite A (not shown here).

Therefore, the activity behaviour of catalyst FHB and FHB mixed with zeolite A were comparable to that of Amberlyst-15. Taking into account that the glycerol etherification with isobutene led to higher selectivity values to h-GTBE, these results are promising for using zeolytic materials for the production of these fuel additives.

4. Conclusions

On the whole, beta catalysts were more active than ZSM-5 and mordenite catalysts in this order for the etherification of glycerol with tert-butanol. This could be related to the number of Brønsted acid sites and their strength together with the accessibility of the reactants to the active sites.

The treatments made on ZSM-5 zeolite practically did not affect its surface and acidic properties, and therefore, similar catalytic behaviour was observed for all ZSM-5 catalysts, which led moderate conversion and very low/null selectivity to h-GTBE.

The lower conversion values and moderate/low selectivity to h-GTBE obtained for mordenite catalysts, when compared with ZSM-5 and Beta catalysts, were related to their lower acid capacity and lower external surface area together with the lower dimensionality and higher hydrophilic character of the mordenite structure.

The incorporation of lanthanum into mordenite and beta zeolites did not improve the catalytic results because of the presence of bulky hydrolysed lanthanum cations blocking the pores, which increased steric hindrances despite the higher strength of the Brønsted acid sites of these catalysts. Desilicated-protonated zeolites also showed lower conversion and lower selectivity to h-GTBE than Na-zeolites despite their slightly higher acidity and higher mesoporosity. This can be explained by the lower strength of their Brønsted acid sites.

Beta catalysts showed the best catalytic results. Fluorinated beta yielded the best conversion (75%) and selectivity to h-GTBE (37%) with the formation of glycerol triether in low amounts. This can due to the higher amounts of stronger acid sites generated because of the incorporation of fluorine in the zeolite framework. Catalytic results of fluorinated beta were comparable to the catalytic activity of Amberlyst-15. This result was improved by mixing fluorinated beta with zeolite A, which adsorbed water from the reaction medium.

From all these results, we can establish that the amount and strength of Brønsted acid sites affects conversion whereas the acidity strength significantly influences the formation of di- and tri-ethers of glycerol. However, the accessibility of the reactants to the acid sites must be guaranteed so that they can act.

Acknowledgments

The authors are grateful for the financial support of the Ministerio de Ciencia e Innovación and FEDER funds (CTQ2008-04433/PPQ). Dolores González acknowledges Ministerio de Educación y Ciencia for a FPU grant (AP2007-03789).

References

[1] M. Pagliaro, R. Ciriminna, H. Kimura, M. Rossi, C. Della Pina, Angew. Chem. Int. Ed. 46 (2007) 4434–4440.
[2] R. D'Aquino, G. Ondrey, Chem. Eng. 114 (2007) 31–37.
[3] J. Feng, M. Yuan, H. Chen, X. Li, Prog. Chem. 19 (2007) 651–658.
[4] A. Behr, J. Eilting, K. Irawadi, J. Leschinscki, F. Lindner, Green Chem. 10 (2008) 13–30.
[5] J. Barrault, F. Jerome, Eur. J. Lipid Sci. Technol. 110 (2008) 825–830.
[6] M. Pagliaro, R. Ciriminna, H. Kimura, M. Rossi, C. Della Pina, Eur. J. Lipid Sci. Technol. 111 (2009) 788–799.
[7] N. Rahmat, A.Z. Abdullah, A.R. Mohamed, Renew. Sustain. Energy Rev. 14 (2010) 987–1000.
[8] M.O. Guerrero-Pérez, J.M. Rosas, J. Bedia, J. Rodríguez-Mirasol, T. Cordero, Recent Pat. Chem. Eng. 2 (2009) 11–21.
[9] T.S. Viinikainen, R.S. Karinen, A.O. Krause, in: G. Centi, R.A. van Santen (Eds.), Conversion of Glycerol into Traffic Fuels Catalysis for Renewables: From Feedstock to Energy Production, Wiley-VCH Verlag GmbH and Co. KgaA, Weinheim, 2007.
[10] F.J. Liotta Jr., L.J. Karas, H. Kesling, US Patent 5,308,365 to ARCO Chemical Technology, L.P. (1994).
[11] M. Marchionna, R. Patrini, D. Sanfilippo, A. Paggini, F. Giavazzi, L. Pellegrini, Stud. Surf. Sci. Catal. 136 (2001) 489–494.
[12] R.S. Karinen, A.O.I. Krause, Appl. Catal. A: Gen. 306 (2006) 128–133.
[13] K. Klepáčová, D. Mravec, E. Hájeková, M. Bajus, Petrol. Coal 45 (2003) 54–57.
[14] K. Klepáčová, D. Mravec, M. Bajus, Appl. Catal. A: Gen. 294 (2005) 141–147.
[15] K. Klepáčová, D. Mravec, A. Kaszony, M. Bajus, Appl. Catal. A: Gen. 328 (2007) 1–13.
[16] J.A. Melero, G. Vicente, G. Morales, M. Paniagua, J.M. Moreno, R. Roldán, A. Ezquerro, C. Pérez, Appl. Catal. A: Gen. 346 (2008) 44–51.
[17] J.A. Melero, J. Iglesias, G. Morales, Green Chem. 11 (2009) 1285–1308.
[18] M. Di Serio, L. Casale, R. Tesser, E. Santacesaria, Energy Fuels 24 (2010) 4668–4672.
[19] H.J. Lee, D. Seung, K.S. Jung, H. Kim, I.N. Filimonov, Appl. Catal. A: Gen. 390 (2010) 235–244.
[20] L. Xiao, J. Mao, J. Zhou, X. Guo, S. Zhang, Appl. Catal. A: Gen. 393 (2011) 88–95.
[21] W. Zhao, B. Yang, C. Yi, Z. Lei, J. Xu, Ind. Eng. Chem. Res. 49 (2010) 12399–12404.
[22] P.M. Slomkiewicz, Appl. Catal. A: Gen. 313 (2006) 74–85.
[23] R. Luque, V. Budarin, J.H. Clark, D. Macquarrie, Appl. Catal. B: Environ. 82 (2008) 157–162.
[24] F. Frusteri, F. Arena, G. Bonura, C. Cannilla, L. Spadaro, O. Di Blasi, Appl. Catal. A: Gen. 367 (2009) 77–83.
[25] N. Ozbay, N. Oktar, N.A. Tapan, Int. J. Chem. React. Eng. 8 (A18) (2010) 1–10.
[26] C. Breen, Clay Miner. 26 (1991) 487–496.
[27] R. Mokaya, W. Jones, S. Moreno, G. Poncelet, Catal. Lett. 49 (1997) 87–94.
[28] J.A. Ballantine, J.H. Purnell, J.M. Thomas, Clay Miner. 18 (1983) 347–356.
[29] M.E. Jamróz, M. Jarosz, J. Witowska-Jarosz, E. Bednarek, W. Tecza, M.H. Jamróz, J.C. Dobrowolski, J. Kijenski, Spectrochim. Acta A 67 (2007) 980–988.
[30] B. Imelik, J.C. Vedrine, Catalyst Characterization, Physical Techniques for Solid Materials, Plenum Press, New York, 1994.
[31] M. Müller, G. Harvey, R. Prins, Microporous Mesoporous Mater. 34 (2000) 135–147.
[32] A.A. Gabrienko, I.G. Danilova, S.S. Arzumanov, A.V. Toktarev, D. Freude, A.G. Stepanov, Microporous Mesoporous Mater. 131 (2010) 210–216.
[33] M. Dolores González, Y. Cesteros, P. Salagre, Microporous Mesoporous Mater. 144 (2011) 162–170.
[34] S. Hayashi, N. Kojima, Microporous Mesoporous Mater. 141 (2011) 49–55.
[35] J.M. Newsam, et al., Proc. R. Soc. London Ser. A 420 (1988) 375–405.
[36] W.M. Meier, Z. Kristallogr. 115 (1961) 439–450.
[37] D.M. Roberge, H. Hausmann, W.F. Hölderich, Phys. Chem. Chem. Phys. 4 (2002) 3128–3135.
[38] V. Paixão, A.P. Carvalho, J. Rocha, A. Fernandes, A. Martins, Microporous Mesoporous Mater. 131 (2010) 350–357.
[39] J.C. Groen, S. Abelló, L.A. Villaescusa, J. Pérez-Ramírez, Microporous Mesoporous Mater. 114 (2008) 93–102.

[40] B.O. Dalla Costa, C.A. Querini, Appl. Catal. A: Gen. 385 (2010) 144–152.
[41] C. Sievers, J.S. Liebert, M.M. Stratmann, R. Olindo, J.A. Lercher, Appl. Catal. A: Gen. 336 (2008) 89–100.
[42] J.A. Van Bokhoven, A. Roest, D.C. Konigsberger, J.T. Miller, G.H. Nachtegaal, A.P.M. Kentgents, J. Phys. Chem. B 104 (2000) 6743–6754.
[43] R.B. Borade, A. Clearfield, J. Chem. Soc. Faraday Trans. 91 (1995) 539–547.
[44] J.P. Marques, I. Gener, P. Ayrault, J.C. Bordado, J.M. Lopes, F.R. Ribeiro, M. Guisnet, C. R. Chim. 8 (2005) 399–410.
[45] F. Ancilloti, F. Mauri, E. Pescarollo, J. Catal. 46 (1977) 49–57.
[46] A. Gicquel, B. Torck, J. Catal. 83 (1983) 9–18.